High-resolution *in situ* measurements of phytoplankton photosynthesis and abundance in the Dutch North Sea

Hedy M. Aardema[1,2], Machteld Rijkeboer[1], Alain Lefebvre[3], Arnold Veen[1], and Jacco C. Kromkamp[4]

[1]Laboratory for Hydrobiological Analysis, Rijkswaterstaat (RWS), Zuiderwagenplein 2, 8224 AD Lelystad, The Netherlands
[2]Department of Climate Geochemistry, Max Planck Institute for Chemistry, Hahn-Meitner-Weg 1, 55128 Mainz, Germany
[3]Ifremer, Laboratoire Environnement et Ressources, BP 699, 62321 Boulogne sur Mer, France
[4]Department of Estuarine and Delta Systems, NIOZ Royal Netherlands Institute for Sea Research and Utrecht University, P.O. box 140, 4400 AC Yerseke, The Netherlands

Correspondence to: Hedy M. Aardema (hedy.aardema@mpic.de),

Abstract. Marine waters can be highly heterogeneous both on a spatial and temporal scale, yet monitoring is currently based on low-resolution methods leading to potential undersampling in time and space. This study explores the potential of two high-resolution *in situ* methods for monitoring of phytoplankton dynamics; Fast Repetition Rate fluorometry (FRRf) for information on phytoplankton photosynthesis and productivity and scanning flowcytometry (FCM) for information on phytoplankton abundance and community composition. These instruments were deployed during four cruises on the Dutch North Sea in April, May, June and August of 2017. The high-resolution methods were able to visualize both the spatial and seasonal variability of the phytoplankton community in the Dutch North Sea. Spectral cluster analysis was applied to objectively interpret the multitude of parameters and visualize potential spatial patterns. This resulted in identification of biogeographic regions with distinct phytoplankton communities, which varied per cruise. Our results clearly show that the sampling based on fixed stations do not give a good representation of the spatial patterns, showing the added value of our approach. Still, to fully exploit the potential of the tested high-resolution measurement set-up, some major improvements can still be made. Among which the most important are; accounting for the diurnal cycle in photophysiological parameters concurrent to the spatial variation, better predictions of the electron requirement for carbon fixation to estimate gross primary productivity, and the identification of more flowcytometer clusters with informative value. Nevertheless, the richness of additional information provided by high-resolution methods such as the FCM and FRRf, can improve existing low-resolution monitoring programs towards a more precise and ecosystemic ecological assessment of the phytoplankton community and productivity.

KEY WORDS: Fast Repetition Rate fluorometry, flow cytometry, phytoplankton photosynthesis, spatial variability, primary productivity

1 Introduction

The Dutch North Sea is of major socio-economic importance because of its close proximity to densely populated areas and the intensive utilization for shipping, fishing, sand extraction and development of offshore windmill farms. Due to this high anthropogenic pressure, the North Sea has undergone considerable biogeochemical and biological changes in the past decades (Burson et al., 2016; Capuzzo et al., 2015 and 2017). For example, nutrient load and stoichiometry were fluctuating substantially due to inflow of wastewater and agricultural run-off and subsequent mitigation efforts (Burson et al., 2016; Philippart et al., 2000). Additionally, water clarity in large parts of the North Sea decreased during the 20th century (Capuzzo et al., 2015). These abiotic changes affect primary productivity and community composition shifts throughout the trophic levels, with large implications for ecosystem functioning and fisheries production (Capuzzo et al., 2017; Burson et al., 2016). Over time, large changes are expected due to the planned energy transition and under the impact of climate change. Anticipated climate change effects include ocean acidification, sea level rise, and increasing temperatures. Already, the North Sea is warming more rapid than most other seas (Philippart et al., 2011). These changing environmental conditions will have a big impact on marine biogeochemistry and thereby on phytoplankton community composition and primary productivity (Sarmiento et al., 2004; Behrenfeld et al., 2006; Marinov et al., 2010). Changes in phytoplankton community composition and primary productivity affect the entire ecosystem and global biogeochemical cycles (Montes-Hugo et al., 2009; Falkowski et al., 1998; Schiebel et al., 2017). Systematic and sufficient monitoring of these changes is of crucial importance to recognize threats, and, once identified as such, develop mitigation actions.

Although phytoplankton community composition and productivity can be highly variable on a spatial and temporal scale, governmental monitoring still consists mainly of low-resolution measurements (Baretta-Bekker et al., 2009; Kromkamp and van Engeland, 2010; Cloern et al., 2014; Rantajarvi et al., 1998). Currently, biological monitoring of phytoplankton in the Dutch North Sea is dictated by the requirements set by OSPAR and the EU Marine Strategy Framework Directive (MSFD 2008/56/EC). It consists of HPLC analysis of Chl *a* concentration and microscopy counts of *Phaeocystis* cells and, at some stations, coccolithophores or toxic dinoflagellates. Sampling points were reduced from almost 70 in 1984 to less than 20 today, while strong seasonal patterns, high riverine input, and tidal forces make the Dutch North Sea a region with high spatiotemporal variability. Modern automated flow-through systems offer the opportunity to record the surface ocean with high spatial and temporal resolution, which has potential to be an effective addition to monitoring programs. Such high-resolution methods are well established in physical oceanography but for biological parameters, the implementation has been lacking. This is mostly due to the complicated interpretation of biological parameters, resulting in high uncertainties in the current global estimates of net primary productivity (Silsbe et al., 2016). Automated flow-through methods are not able to replace some more detailed low-resolution measurements, but their higher spatial and temporal resolutions provide the possibility to identify short-lived events and act as an early warning system. Additionally, because the measurements are done *in situ*, it is possible to acquire information on rates of living organisms and samples unaffected by transport, storage or conservation. Two non-invasive,

high-resolution methods that can be used in phytoplankton monitoring programs are scanning flowcytometry (FCM) for information on phytoplankton abundance and community composition and Fast Repetition Rate fluorometery (FRRf) to give information on phytoplankton photophysiology. Scanning flowcytometry is a method for counting and pulse-shape recording of phytoplankton cells resulting in a high number of parameters on size, fluorescence and scattering properties per algal cell. Based on these characteristics cluster analysis allows for division into groups of similar pigment characteristics and size classes (Thyssen et al., 2015). The FRRf uses active fluorescence to gain insight into phytoplankton photophysiology. This technique is an alternative to the traditional production-light curves (PE-curves) by measuring the photosynthetic electron transport rate (or gross photosynthesis) at increasing ambient light levels (Suggett et al., 2009a; Silsbe and Kromkamp, 2012). Electron transport rate per unit volume is estimated by a series of single turnover light flashes that cumulatively close all photosystems (Kromkamp and Forster, 2003; Suggett et al., 2003). This single turnover technique allows for calculation of the effective absorption cross-section and, in combination with an instrument specific calibration coefficient, the absorption coefficient and amount of reaction centres per volume (Kolber et al, 1998; Kromkamp and Forster, 2003; Oxborough et al., 2012; Silsbe et al., 2015). Electron transport rate per unit volume is used to estimate gross primary productivity (Kromkamp et al., 2008; Smyth et al., 2004; Suggett et al., 2009a). These two methods are supplementary, because the interaction of phytoplankton with their environment is always a sum of the community composition and their physiology. For instance, if waters become more turbid, phytoplankton can acclimate by increasing their effective absorption cross section, but it could also lead to a shift in community composition toward species with higher light use efficiency (Moore et al., 2006).

The aim of this study is to test the suitability of these two high-resolution methods to be developed as novel phytoplankton monitoring method. The two high-resolution methods, a flowcytometer and a FRR fluorometer, were deployed concurrently on four 4-day cruises in April, May, June and August to meet a wide range of environmental conditions and phytoplankton community states. These measurements allow for quantification of seasonal and mesoscale spatial patterns in phytoplankton abundance, photophysiology and gross primary production. In this paper we provide an overview of the acquired results, use a spectral cluster analysis to visualize spatial heterogeneity and evaluate the potential of these methods to optimize current monitoring programs.

2 Methods

2.1 Study site and sampling

The Dutch North Sea is a shallow tidal shelf sea in the southern part of the North Sea. The main water flow is northward. Atlantic water enters the North Sea from the south via the Channel and from the northeast where it curves around Scotland. Both currents meet north of the Dutch coast forming the Frisian Front. For a detailed description on the North Sea physical oceanography, see Sündermann and Pohlman (2011). Along the Dutch coast, high river input from especially the Rhine River decrease the salinity and loads the coastal zone with high nutrient concentrations (Burson et al., 2016). Anthropogenic pressure is high in the Dutch North Sea resulting in a history of large shifts in nutrient concentrations and water clarity (Capuzzo et al., 2015; Burson et al., 2016).

The monitoring of the Dutch North Sea is performed by the Dutch government (Rijkswaterstaat) in a monitoring program called MWTL (Monitoring Waterstaatkundige Toestand des Lands, freely translated as 'Monitoring of the status of the governmental waters of the country'). The location of the sampling stations of the program are organized along transects (Fig. 1). The stations are sampled between March and October with a frequency of every two or four weeks, dependent on the transect.
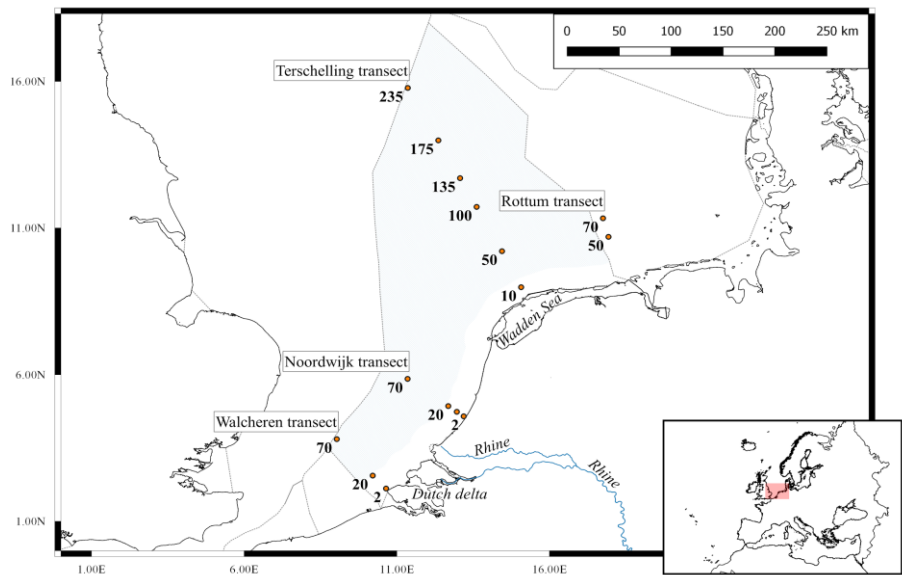

Figure 1: Sampling locations of the MWTL monitoring program referred to in this study. The stations are named according to the transect (Terschelling, Noordwijk and Walcheren), followed by the amount of kilometres from the coast (labels next to sampling points). The boundaries of the Exclusive Economic Zone (EEZ) are indicated by the grey dotted lines and the Dutch EEZ is coloured light blue. The locations of three major infows to the Dutch North Sea are named at the corresponding locations (Rhine river, Dutch Delta and the Wadden Sea). Insertion visualizes the location of the Dutch North Sea in a broader map of Europe.

In 2017, four 4-day sampling surveys (10-13 April, 15-18 May 12-15 June and 14-17 August), were conducted for the JERICO-NEXT project on board the RV *Zirfaea* during their regular monitoring cruises on the Dutch North Sea. To assess the heterogeneity of the Dutch North Sea and the benefits associated with high-resolution monitoring the four cruises were conducted in different months (April, May, June and August), thereby aiming to cover different seasons and stages of the phytoplankton bloom (Baretta-Bekker et al., 2009).

On the RV *Zirfaea* the water inlet was situated approximately 3.5 m below sea surface level. From the water inlet the sample water, with a flow rate of approximately 24 litres per minute, was split towards 1) a flow-through -4H-JENA Ferrybox (-4H-JENA engineering GmbH, Germany) equipped with an FSI Excell® Thermosalinograph (Sea-Bird Scientific, USA) to measure temperature and salinity and a SCUFA™ Submersible Fluorometer (Turner Designs Inc., USA), and 2) at a flow rate of 1 L per minute towards a 230 cm^3 flow through sampling container where water was cleared from bubbles and sand. The time from water inlet to sampling chamber was approximately 2 minutes. A FastOcean Fast Repetition Rate fluorometer (FRRf) with Act2-based laboratory flow through system (Chelsea Technologies Group Ltd, UK) and a Cytosense scanning flowcytometer (Cytobuoy BV, the Netherlands) automatically sampled from the sampling unit every 30 minutes. Since the average speed of the ship was 8 knots, the average spatial resolution of FCM and FRRf measurements was on average 7.5 kilometres. The Ferrybox sensors stored data every minute. During the cruises the high-resolution methods (FRRf, FCM and Ferrybox) were combined with lower resolution methods, consisting of measurements at 13 to 19 stations. At these stations surface samples were taken for nutrient and chlorophyll *a* analyses (see 2.2 chemical analyses) using a rosette sampler equipped with a CTD and Niskin bottles.

2.2 Chemical analyses

Samples for nutrient analyses were filtered over Whatmann GF/F filters and kept frozen until analyses. The analyses of ammonium (NH_4^+), nitrite (NO_2^-), nitrate (NO_3^-), ortho-phosphate (PO_4) and silicate (Si) concentrations were conducted by the Rijkswaterstaat laboratory (the Netherlands) according to ISO 13395, 15681, 16264 using a San^{++} Analyzer (Skalar Analytical B.V., the Netherlands). In the RWS internal protocol, nitrite+nitrate is measured by first reducing nitrate to nitrite using a cadmium/copper column and addition of ammoniumchloride as a buffer. Thereafter, sulphanilamide, α-naphthyl ethylenediamine dihydrochloride and phosphoric acid are added and the extinction at 540 nm compared to a $NaNO_2$ standard. For measurement of Ammonium concentrations first EDTA was added to bind Calcium and Magnesium. Then, sodium salicylate, sodium nitroprusside and sodium hypochlorite were added and the extinction at 630 nm compared to a NH_4Cl standard. Ortho-phosphate was measured by adding molybdate reagent and ascorbic acid to the sample and led through an oilbath at 37 ± 2 °C. Followed by measuring the extinction at 880 nm and comparing to a standard. Silicate concentration was measured by subsequent addition of molybdate reagent, oxalic acid and ascorbic acid. The silicate concentration was then

determined by measuring the extinction at 810 nm and comparing to a silicate standard. The detection limits of the nutrient analyses were: NO_3NO_2: 0.7 µM, Si: 0.36 µM and PO_4^{3-}: 0.03 µM.

Chlorophyll *a* concentration (hereafter Chl *a*) was determined by filtering over Whatmann GF/C filters and freezing the filter at -80 ºC. The Chl *a* was extracted in 20 ml 90% acetone and centrifuged for 15 minutes with glass pearls (1.00-1.05 mm) using a Bullet Blender Tissue homogenizer (Next Advance, Inc., Troy, USA) under cooling of solid CO_2. The extract was analysed in duplicates using Ultra High Performance Liquid Chromatography (UHPLC). The calibration of the UHPLC system is performed every analysis day by making a 12-point standards calibration curve calculated using quadratic regression with weighting method 1/A to better distinguish smaller peaks (R^2>0.995). The injection volume was 20 µl, unless the concentration was below the lowest standard, in which case a second injection of 40 µl was reanalysed. The analysis was conducted by the MUMM laboratory (Belgium) using according to RWS analysis protocol A200. Quality control was performed by the RWS laboratory (The Netherlands).

2.3 High frequency methods

2.3.1 Variable fluorescence

Variable fluorescence was measured with a FastOcean Fast Repetition Rate fluorometer (FRRf) and Act2-based laboratory system (Chelsea Technologies Group Ltd, UK). Temperature was controlled by connecting a Lauda ecoline cooler (LAUDA-Brinkmann, LP., USA) to the water jacket of the Act2 system.

The acquisition protocol consisted of 100 excitation flashes with a flash pitch of 2 µs and 40 relaxation flashes with a flash pitch of 60 µs. Excitation flashes were performed with the blue LED (450 nm) and strength of the LEDs was automatically adjusted to the phytoplankton concentration by the manufacturer' FAstPro software. A loop of simultaneous blue and green flashes (450 nm+530nm) was performed after the acquisition loop of only blue LEDs in case the blue LEDs were not able to reach saturation (for instance with high cyanobacteria concentrations), but as this was not the case, only the parameters measured by blue LEDs were used for further calculation. The sequence was repeated 20 times with a sequence interval of 100 ms. The sample was refreshed before each fluorescent light curve (FLC) by flushing for 60 seconds and kept well-mixed by "flushing" for 200 ms between acquisition loops.

The FLC protocol consisted of 14 light steps of 100 s, of which the light intensity was automatically adjusted to get the optimal FLC shape based on the previous light curve. A pre-illumination step (55 seconds on 12 µmol photons m^{-2} s^{-1}) was included before the FLC to low light acclimate the phytoplankton and to relax non-photochemical quenching (NPQ) of diatoms and other chlorophyll *a-c* algae as they stay in the light activated state in the dark (Goss et al., 2006). After each light step, measurements were made in the dark for 18s to retain a value for F_0' (minimal fluorescence in light acclimated state). The data

were corrected for the background fluorescence by taking sample blanks multiple times per day by filtration over a 0.45 µm filter and subtracting the last determined background fluorescence from the sample fluorescence.

An overview of the derived photosynthetic parameters can be found in Table 1. To derive values for the maximum photosynthetic electron transport rate (P_{max}), minimum saturating irradiance (E_k) and the light utilisation efficiency (α) the relative electron transport rate (rETR) of the samples was fitted to the exponential model of (Webb et al. 1974), after normalizing the data to the irradiance as described by (Silsbe and Kromkamp, 2012):

$$F_q'/F_m' = \frac{P_{max}\left(1-\exp\left(\frac{-E}{E_k}\right)\right)}{E} \tag{1}$$

where E is the irradiance in µmol photons m^{-2} s^{-1}, F_q'/F_m' the effective PSII quantum efficiency, α is the initial slope of the rETR vs irradiance curve and E_k is the light saturation parameter (in µmol photons m^{-2} s^{-1}). The relative maximum rate of photosynthetic electron transport (P_{max}) was calculated as:

$$P_{max} = E_k \times \alpha \tag{2}$$

Table 1: The derived photosynthetic parameters used in the text (see Oxborough et al. (2012) and Silsbe et al. (2015) for more information). Variables used in equation 1-8 are not included but discussed in the text.

	Description	unit
Parameters derived from fluorescence induction curve		
F_0	Minimum fluorescence, measured at zeroth flashlet of an FRRf single turnover measurement when all PSII reaction centers (RCII) are open. Estimate for chlorophyll *a* concentration.	Dimensionless
F_m	Maximum fluorescence, reached at nth flashlet of an FRRf single turnover measurement when all PSII reaction centers are closed.	Dimensionless
$1/\tau$	Rate of re-opening of a closed RCII	ms^{-1}
σ_{PSII}	Effective absorption cross section of PSII photochemistry	nm^2 $PSII^{-1}$
Parameters calculated from parameters derived from fluorescence induction curve		
JV_{PII}	PSII charge separation rate per unit volume (see eq. [3])	µmol electrons m^{-3} h^{-1}
F_v/F_m	Quantum efficiency of PSII under dark conditions (see eq. [4])	Dimensionless
a_{LHII}	Absorption coefficient of PSII light harvesting (see eq. [5])	m^{-1}
[RCII]	Functional PSII reaction centers per volume (see eq. [6])	nmol RCII m^{-3}
Parameters derived from Fluorescence light curve (FLC)		
α_{PSII}	Initial slope of the FLC, an estimate of affinity for light	µmol electrons (µmol photons) $^{-1}$
E_k	Minimum saturating irradiance of fluorescence light curve	µmol photons m^{-2} s^{-1}
P_{max}	Maximum photosynthetic electron transport rate	µmol electrons m^{-2} s^{-1}
Parameters calculated from parameters derived from fluorescence light curve and irradiance		
Surface GPP	Surface Gross Primary Productivity (see eq. [3]) calculated based on the FLC-parameters and incoming irradiance.	µg C L^{-1} h^{-1}

7

The PSII flux in μmol electrons m^{-3} h^{-1} was calculated as the product of the effective PSII efficiency (F$_q$'/F$_m$'), the optical absorption cross section of the light harvesting pigments of PSII (a$_{LHII}$) and the irradiance (E):

$$JV_{PII}(\text{ in } \mu mol \text{ electrons } (PSII \text{ } m^{-3}) \text{ } h^{-1}) = F_q'/F_m' * a_{LHII} * E \tag{3}$$

where

$$F_q'/F_m' = \frac{F_m' - F'}{F_m'} \tag{4}$$

and

$$a_{LHII} \text{ } (in \text{ } m^{-1}) = \frac{F_0 * F_m}{F_m - F_0} * K_a \tag{5}$$

K$_a$ (m^{-1}) is an instrument specific factor necessary for obtaining absolutes rate of photosynthetic transport (see Oxborough et al. (2012) and Silsbe et al. (2015) for more information). The amount of reaction centres per cubic metre ([RCII]) was calculated as

$$[RCII] \text{ } (in \text{ } nmol \text{ } m^{-3}) = K_a * \frac{F_0}{\sigma_{PSII}} \tag{6}$$

for more information on the calculation of [RCII] and a$_{LHII}$ see Oxborough et al. (2012) and Silsbe et al. (2015).

Q$_A$ reoxidation or rate of re-opening of a closed RCII was calculated as 1 divided by the time constant of re-opening of a closed RCII with an empty Q$_B$ site (τ$_{ES}$) in ms^{-1}.

Standardized daily anomalies (Z-scores) were calculated for the photophysiological parameters as:

$$Z - score = \frac{x - daily \text{ } mean(x_0 ... x_{24})}{Daily \text{ } standard \text{ } deviation(x_0 ... x_{24})} \tag{7}$$

Partial days were excluded because this could potentially offset the daily mean and standard deviation.

Gross Primary Productivity (GPP) was estimated by fitting JVPII in μmol photons m^{-3} h^{-1} to equation 1 (the exponential model of Webb et al., 1974) to derive a volumetric P$_{max}$ and α. GPP in μg C L^{-1} h^{-1} was then calculated using equation 1 and incident surface irradiance. To avoid effects of changing incident surface irradiance (E$_{surface}$) on the spatial pattern and to be able to compare GPP between regions we used monthly average surface irradiances (E$_{surface}$) in our calculations of primary productivity. From 2010-2016 irradiance (400-700 nm) was measured at the roof of the NIOZ building in Yerseke using a LI-190 quantum PAR sensor and hourly averages stored using a LI1000 datalogger. E$_{surface}$ was then calculated by averaging all irradiance data from the years 2010-2016 for the respective month. The primary productivity in electrons units was converted to carbon units by assuming 6 moles of electrons were required to fix one mole of carbon, based on a study in the adjacent Oosterschelde and Westerschelde estuaries (Kromkamp et al., in prep.).

2.3.2 CytoSense scanning flowcytometry

Single cell measurements of the phytoplankton community were conducted using a bench-top scanning flowcytometer (Cytobuoy BV, the Netherlands) equipped with two lasers (488 nm and 552nm; 60mW each). Both laser beams were ca. 5 µm high and 300 µm wide and were focussed on the same spot in the middle of the flow-through chamber. The speed of the particles was ca. 2.2 m s^{-1}. The system contained 3 fluorescence detector channels separating fluoresced wavelengths of 550-600 nm (FLY; Phycoerythrin), 600-650 nm (FLO; Phycocyanin) and above 650 nm (FLR; chlorophyll *a*). Additionally, the Forward light Scatter (FWS) and Sideward light Scatter (SWS) of all particles was measured. The FCM was equipped with a double set of detectors (PMT's) for each of the three fluorescence channels to increase the dynamic range (Rutten, 2015). Per cell the pulse shape recording and the parameters (FWS, SWS, FLR, FLO and FLY) plus their affiliates (length, total and maximum values) were recorded and saved. The instrument was checked daily for drift using 3 µm Cyto-Cal^{TM} 488 nm alignments beads (Thermo Fisher Scientific Inc., USA). Additionally, the FCM was equipped with an Image-in-flow camera to take pictures of the nano- and micro-phytoplankton. This allows for linking pulse shape recordings to microscopy results and thereby identification of represented phytoplankton groups in respective clusters.

Phytoplankton cells were clustered based on the pulse shape recording of the individually scanned phytoplankton. In this paper we discriminate the phytoplankton groups based on their size (pico, nano and micro) and Orange/Red fluorescence ratio (hereafter O/R ratio; Table 2). The chosen cluster criteria were based on expert judgement (SeaDataNet, 2018) and corresponding to other studies (Sieburth et al., 1978; Vaulot et al., 2008). The clustering was done by the software Easyclus 1.26 (ThomasRuttenProjects, The Netherlands) according to these criteria. Noise, air bubbles and other potential outliers were removed. Size was calculated based on the length FWS. Due to the speed acceleration of the particles in the sheath fluid of the FCM the organisms will flow along their long axis, which makes the FWS a good estimate of the length of the particles. We obtained a linear relation between Length FWS and measured length of diverse phytoplankton species, having an angle of inclination of almost 1 and R^2 =0.98 (Rijkeboer, 2018). For organisms smaller than 5 µm there may be some deviation from this relationship due to the width of the laser beam (which is 5 µm).

Table 2: The phytoplankton groups distinguished in the current study.

Name	Cluster criteria		Main corresponding taxonomic group(s)
	Length FWS	O/R-ratio	
Pico-Red	<4 µm*	<1	Pico-eukaryotes
Pico-Synecho	<4 µm*	>1	ynechococcus
Nano-Crypto	4-20 µm	>1	Cryptophycea
Nano-Red	4-20 µm	<1	Diatoms,Haptophytes, Dinoflagelates
Micro-Red	>20 µm	<1	Diatoms,Haptophytes, Dinoflagelates

*In june <6 µm

2.4 Data analysis

Outliers of the complete dataset were removed after visual inspection of pairplots made with the pairplot function of the HighstatLib.V4 script (Zuur et al., 2009). For the FRRf data, the fitted FLC curves were visually inspected for a good fit and removed based on expert judgement, which led to removing 1% to 7% of the FLC fits. Especially at low biomass FLCs became noisy, therefore a minimum fluorescence signal was set for calculations of photosynthetic parameters. Below this blank corrected instrument-specific fluorescence signal F_q'/F_m' became noisy and often reached above the biologically unlikely limit of 0.65 (Kolber and Falkowski, 1993). The datasets of the high-resolution measurements (FRRf, FCM and Ferrybox) were linked using corresponding timestamps. When multiple measurements were performed within one FLC, the average was used. To find regions with similar phytoplankton communities, data was spectrally clustered using the uHMM R package (Poisson-caillault and Ternynck, 2016) in the statistical software R (version 3.4.1, R Core Team, 2017). The package default settings normalize data before clustering, and automatically find the number of clusters based on spectral classification and the geometry of the data. This new methodology is more robust than the classical hierarchical and k-means technics (Rousseeuw et al., 2015). Phytoplankton parameters were first tested for collinearity and predictors with a variance inflation factor (VIF) over 6 were removed (Zuur et al., 2009; see supplementary material for pairplots). This left for the cluster analysis FCM-parameters Pico-red, Nano-red, Micro-red and *Synechococcus* and the FRRf-parameters σ_{PSII}, F_v/F_m, a_{LHII}, $1/\tau$, E_k. Datapoints were then per cluster labelled and plotted on a map to visually identify regions. Principal Component Analyses (PCA) were performed to find which variables contributed most to the cluster results The PCA's were based on correlation matrixes with scaled parameters to correct for unequal variances and was carried out with the prcomp() function in R (version 3.4.1, R Core Team, 2017). The PCA visualization was done using the supplemental R package factoextra (Kassambra and Mundt, 2017). Maps were made using QGIS v. 2.14.2 and other figures were made with ggplot2 in R (Wickham, 2009).

3 Results

3.1 Abiotic conditions

Environmental conditions in the Dutch North Sea are spatially heterogeneous and strongly influenced by seasonal dynamics. Sea surface temperature increases from 9.5 ± 1.0 °C in April to 19.0 ± 0.6 °C in August (supplementary table S1). Seasonal variations in salinity are small with highest monthly mean salinity in April (34.1 ± 1.8).Spatial variability of salinity is higher with river influx decreasing the salinity down to 26 in the coastal zone. The monthly average of turbidity does show seasonal variation and was higher in April (2.3 ± 3.0 NTU) in comparison to other months. This was reflected in the K_d values, which were also highest in April (0.39 ± 0.28 m^{-1}; supplementary table S1). It needs to be noted that monthly averages are not completely comparable, because of differences in sampling route and stations (Fig. 3).

Dissolved Inorganic Nitrogen (DIN; Nitrate+Nitrite+Ammonium) and silicate (Si) concentrations show both spatial and seasonal variability (Table 3). Spatially, two trends are distinguishable: a coastal-offshore gradient and a longitudinal gradient. The seasonal variability determines the strength and position of these spatial gradients. The coastal to offshore gradient moves shoreward from April to August and the southern stations are depleted earlier in the season in comparison to the more northerly stations. In April DIN and Si concentrations are on average higher and only potentially limiting (Si<1.8 µmol L^{-1}, DIN<2 µmol L^{-1}; Peeters and Peperzak et al. (1990) and references therein) in the most Southerly part of the Dutch North Sea (Walcheren transect) and at offshore stations (>70 km offshore west of the Netherlands, >135 km North of the Netherlands). In later months, DIN and Si limitations gradually moves towards the coastal zone. Stations closest to freshwater influx (Noordwijk 2 and 10) become DIN and Si-limited later in the year (Table 3). The increased DIN concentration at the transect close to the Rhine outflow is absent seventy kilometers offshore (Noordwijk 70), suggesting that the Rhine water remained close to the coast.

Phosphate concentrations were generally quite low and possibly limiting (ortho-phosphate PO$_4^{3-}$<0.5 µmol L^{-1}; Peeters and Peperzak et al, 1990). With exceptions in April north of Terschelling between 50 and 100 km offshore and in May at Noordwijk 2, a region with high freshwater influx. In August phosphate concentrations recovered in the Southern part of the Dutch North Sea reaching up to 0.6 µM. For a table on the N:P ratios see the supplementary table S2.

Table 3: nutrient concentrations (µM) separated per month (April, May, June and August) and station. The stations are named according to name of the transects and the distance in kilometres from the coast (Fig. 1). Potentially limiting nutrient concentrations are shown in red (DIN<2 µmol L^{-1}, Si<1.8 µmol L^{-1}, PO$_4$$^{3-}$<0.5 µmol L^{-1}; Peeters and Peperzak et al, 1990). B.d: below detection limit.

Station	DIN (µM)				PO$_4$$^{3-}$ (µM)				Si (µM)			
	April	May	June	August	April	May	June	August	April	May	June	August
Walcheren 2	1.0	2.4	3.4	1.0	0.2	0.2	0.4	0.6	0.6	0.7	1.4	1.9
Walcheren 20	1.2	3.1	1.1	b.d	0.1	0.1	0.3	0.3	b.d	2.7	0.5	2.0
Walcheren 70	1.1	1.2	1.1	b.d	0.2	0.2	0.2	0.1	b.d	0.6	0.4	0.9
Noordwijk 2	37.5	21.7	4.9	b.d	0.3	0.6	0.2	0.2	6.7	3.5	0.8	1.2
Noordwijk 10	28.5	15.0	3.1	b.d	0.2	0.1	0.4	0.1	2.9	3.2	0.7	1.4
Noordwijk 20	21.6	4.9	0.9	b.d	0.2	0.1	0.2	0.1	1.3	0.7	0.8	0.6
Noordwijk 70	b.d	1.0	0.9	b.d	0.2	0.2	0.3	0.2	b.d	1.1	1.7	0.1
Terschelling 10	10.1	1.9	0.9	b.d	0.3	0.2	0.2	0.2	3.0	2.4	0.5	0.7
Terschelling 50	8.9	b.d	3.4	2.8	0.5	0.2	0.2	0.3	4.6	1.7	2.4	5.0
Terschelling 100	12.6	b.d	1.9	b.d	0.5	0.2	0.3	0.2	3.9	0.5	1.1	1.7
Terschelling 135	1.6	0.8	0.9	b.d	0.4	0.1	0.1	0.3	2.0	0.8	0.9	1.8
Terschelling 175	0.9	NA	1.0	b.d	0.2	NA	0.2	0.2	0.6	NA	0.5	b.d
Terschelling 235	1.0	NA	0.9	b.d	0.2	NA	0.3	0.3	b.d	NA	1.1	0.5

5

10
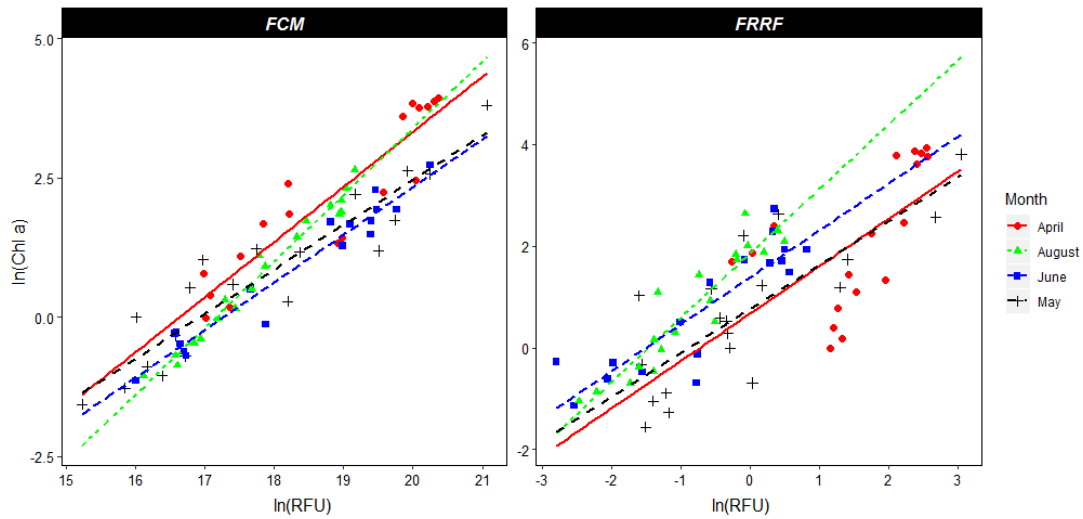
Figure 2: linear regression of the natural logarithms of Chl *a* concentration in µg L^{-1} as determined by HPLC (y-axis) and on the x-axis the natural logarithm of; FCM-derived total red fluorescence (in relative fluorensence units (RFU), left panel) and FRRf-derived minimum fluorescence (F$_0$ in RFU, right panel). Both FCM red fluorescence ($p < 0.01$, adjusted R^2=0.90) and the FRRF F$_0$ ($p < 0.01$, adjusted R2=0.66) are significant predictors for Chl *a* concentrations. The months (April, May, June and August) were a significant predictor of Chl a concentration for both the FRRf ($p < 0.05$) and the FCM ($p < 0.01$). The interaction between the x and y axis was only significant for the FCM data ($p < 0.05$).

3.2 Phytoplankton abundance and fluorescence

High-resolution measurements of phytoplankton presence are based on either cell numbers (flowcytometers) or fluorescence (fluorometers, such as the "standard" chlorophyll sensors, FRRf, and some flowcytometers). Both parameters can yield contrasting results due to the wide range of phytoplankton cell sizes and species-specific Chl a content per cell (Falkowski and Kiefer, 1985; Kruskopf and Flynn, 2005). In this study this is clearly demonstrated by the higher phytoplankton average cell count in June in comparison to April, while the average fluorescence is higher in the latter (supplementary material; Fig. S1). This can be explained by the high relative abundance of pico-phytoplankton, which contributes little to total fluorescence.

Both the FRRf and FCM provide significant predictors of HPLC-derived Chl *a* concentration (Fig. 2). When performing an ANCOVA with month as factorial predictor, natural logarithm transformations were necessary because of the highly unequal variances between months. The ANCOVA with the FRRf-derived F$_0$ as Chl *a* predictor revealed that Chl *a* concentrations significantly differed per month ($p < 0.01$) but not the slope, and that F$_0$ was a significant predictor ($p < 0.01$) of Chl *a* concentration (adjusted R^2=0.66). Yet, the FCM estimate of Chl *a* concentration (TFLR) was a better predictor ($p < 0.01$) with an adjusted R^2 of 0.90. The ANCOVA with the FCM-derived TFLR as Chl *a* predictor resulted not only in a significant difference of the Chl *a* concentration per month ($p < 0.01$) but also in a significantly different slope ($p < 0.05$), suggesting that other predictors that differ per month are influencing the amount of fluorescence per Chl *a* molecule (Fig. 2).

13

Chl *a* concentration is a limited predictor of biomass because the Chl *a* concentration per cell is species-specific and subject to phenotypic acclimation to abiotic conditions (Falkowski and Kiefer, 1985; Kruskopf and Flynn, 2005). Therefore, the FRRf yields other biomass related proxies next to the minimum fluorescence, that allow for circumvention of the use of a chlorophyll a estimate to estimate primary productivity (Oxborough et al., 2012). These parameters are the total absorption coefficient in the water (a_{LHII} in m^{-1}) based on the absorption of the photosynthetic pigments associated with PSII and the amount of PSII reaction centres per volume ([RCII] in nmol RCII m^{-3}). Both are very strongly correlated to F_0, although the ratio of RCII to a_{LHII} can vary by nature, affecting n_{PSII} (Supplementary material; Fig. S3).

3.3 Phytoplankton community composition

Both cell numbers and the phytoplankton community composition showed high spatial heterogeneity in the Dutch North Sea in the sampled months (Fig. 3). In cell numbers, the pico-red group was always present as the dominating group. Because of their low total biovolume, they were contributing less to total red fluorescence. The relative abundance of picophytoplankton was generally higher offshore and in the northern part of the Dutch North Sea. The pico-*Synechococcus* group showed a strong numerical presence offshore in April and in most of the Dutch North Sea in June. The nano-red group was often a dominant group, both in sense of cell numbers as contribution to total red fluorescence. The nano-cryptophytes were never abundant in cell numbers, but contributed to the total red fluorescence in the northern offshore regions. The microphytoplankton group had a low numerical abundance and represented always less than 10% of the total cell counts. Yet in terms of red fluorescence they sometimes dominate, which occurred most frequently in coastal regions (Fig. 3).

In April the northern part of the Dutch North Sea was numerically dominated by picoplankton whereas the southern part and the north coastal area of the Dutch EEZ were numerically dominated by nanophytoplankton. The taxons with high phycoerythrin content (*Synechococcus* and Cryptophycea) made up only a small proportion of the total phytoplankton community in April (generally less than 10%) and were most abundant in the norther part of the Dutch North Sea (Fig. 4e). Microphytoplankton abundance < 3%, and highest numbers were found close to the Dutch Delta and along the Noordwijk transect. The phytoplankton community in May is different from April and occurs very patchy (Fig. 3, second column). Offshore the highest percentages of picophytoplankton were observed (60-80%), whereas the highest percentage of nanophytoplankton was observed north of Terschelling 100 and in the coastal zone. Between May and June the community composition shifted and phytoplankton cell numbers increased. Both groups of pico-phytoplankton (*Synechococcus* and Pico-red) increase in relative abundance between May and June, while the nano-phytoplankton shows a strong decrease (Fig. 3). Highest abundance of pico-phytoplankton was observed offshore. The microphytoplankton is the largest contributor to red fluorescence in the coastal region, although this group does not increase in relative abundance in comparison to May (Fig. 3). In August the pico-phytoplankton was dominating the phytoplankton communities with an average contribution to total cell

numbers of over 80% and only slightly lower values were observed (but still > 70%) along the southern Dutch coast, where the abundance of nano-phytoplankton was higher. Micro-phytoplankton was hardly observed, but because of their high red fluorescence they contributed to total red fluorescence in coastal regions.
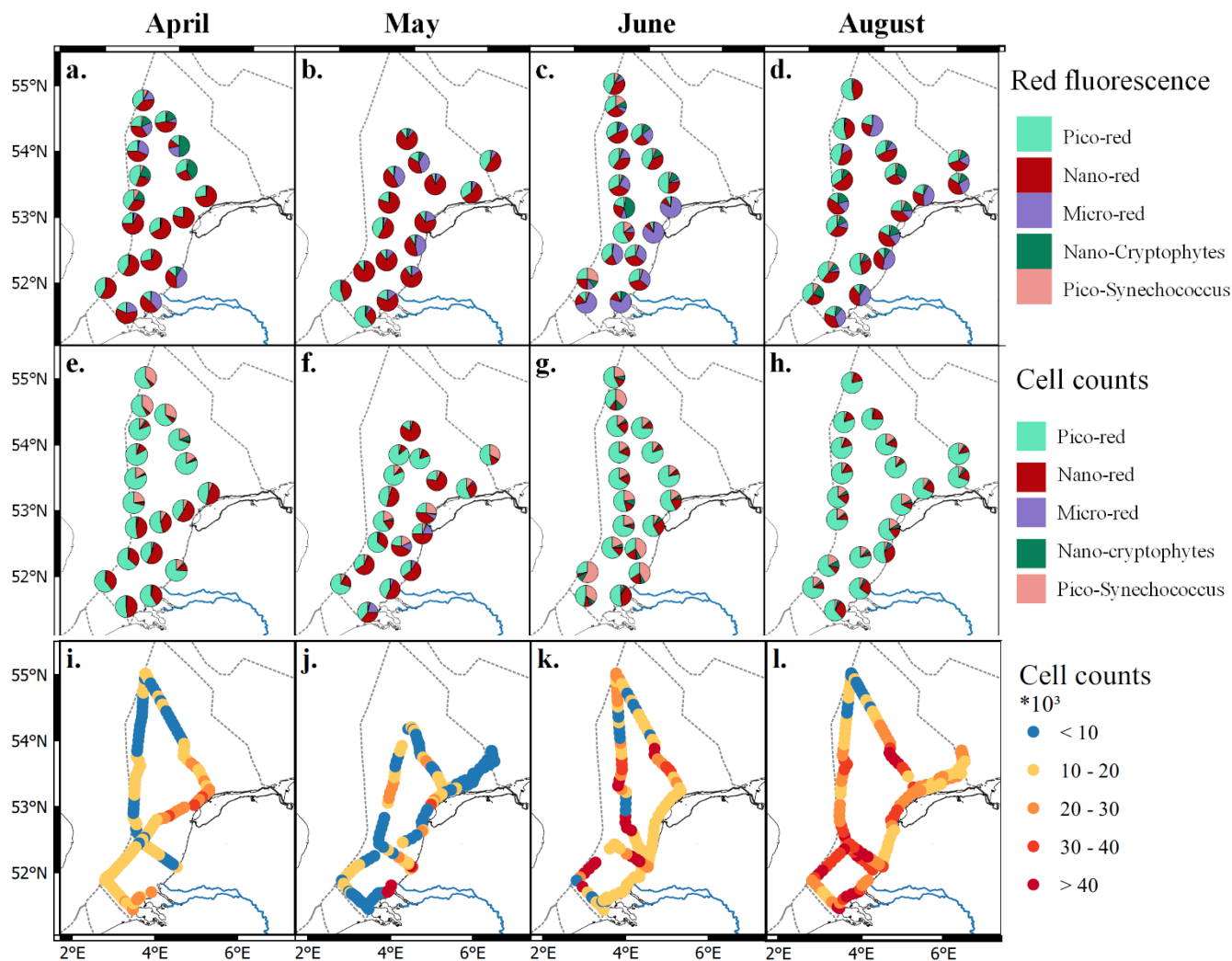
5

Figure 3: Relative phytoplankton community composition using FCM-derived total red fluorescence (first row; a-d) and cell numbers (second row, e-h) in April, May, June and August (from left to right). The groups are clustered according to table 2.

3.4 Photophysiology

Photosynthetic parameters are sometimes highly correlated (Supplementary material; Fig. S3). The correlation of alpha and F_v/F_m, indicators for photosynthetic affinity and photosynthetic efficiency, were, as expected, perfectly correlated (r=1). The parameters derived from the PE-curve, P_{max} and E_k, show high correlation. But surprisingly, α does not show any correlation with E_k. This suggests that the light affinity is not dependent on the level of irradiance where the PSII reaction centres become saturated, or that its value is obscured by nutrient limitation. As expected σ_{PSII}, is very strongly negatively related to n_{PSII} (r=-0.9); the larger n_{PSII}, the smaller the number of pigment molecules associated with it.

In April, the photophysiology of the phytoplankton communities in the Dutch North Sea showed low variability. The F_v/F_m values stayed above 0.5 in northern regions and above 0.4 in southern regions (Fig. 4a). The σ_{PSII} stayed in a narrow range between 2.5-4 nm^2 $PSII^{-1}$ (Fig. 4e). E_k in April showed more variability in comparison to the F_v/F_m and σ_{PSII}, without clear spatial patterns in offshore regions. In the coastal zone, the E_k is lower off the coast from Walcheren and higher off the coast from Noordwijk (Fig. 4i).
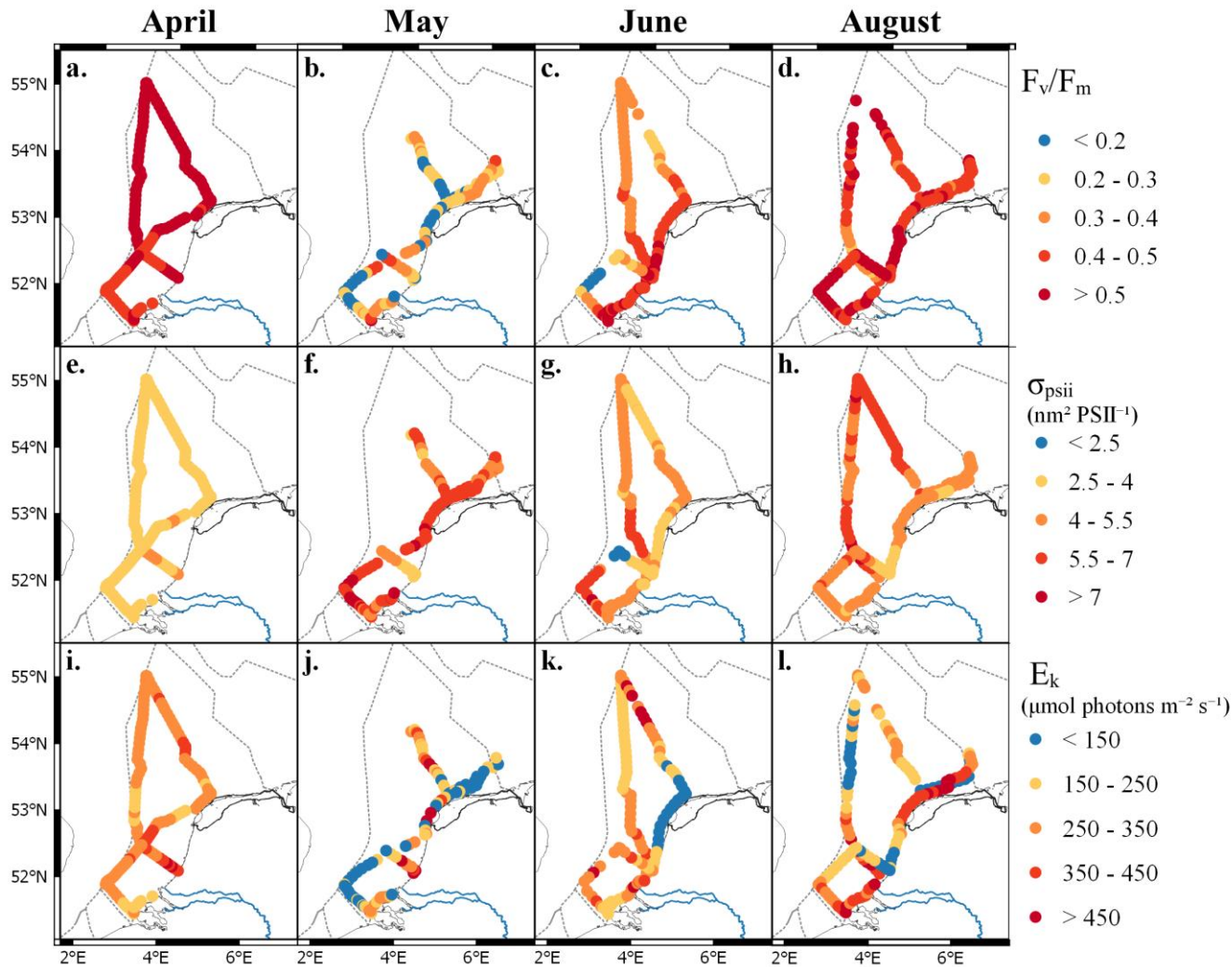
In May photophysiological parameters of the phytoplankton communities in the Dutch North Sea were strongly heterogeneous with only smaller scale spatial patterns (Fig. 4b,f,j). F_v/F_m was in general much lower in May (0.1-0.5) than in April (>0.4) across most of the Dutch EEZ (Fig. 4b). The range in σ_{PSII} was larger in May in comparison to April (Fig. 4f). The σ_{PSII} was also higher across the Dutch North Sea, except from a small area near the coast of Noordwijk. A possible consequence of the outflow of the Rhine River. In the same region the E_k is high (> 450 μmol photons m^{-2} s^{-1}), but in other regions where E_k is high this does not coincide with an increased σ_{PSII}. The E_k across the Dutch North Sea in May is heterogeneous without large-scale spatial patterns.

In June the photophysiology of the phytoplankton in the Dutch North Sea is still as heterogeneous as in May, but larger scale spatial patterns seem to occur. The F_v/F_m values recovered to above 0.4 in the coastal zone, but not in offshore regions in the Southern North Sea. The F_v/F_m of the southern offshore phytoplankton, between Walcheren 70 and Noordwijk 70 (Fig. 1), remained lowest (<0.2; Fig. 4c). The σ_{PSII} was lower than in May, apart from the southern offshore region that remained higher (Fig. 4g). In a small region around Noordwijk 70 the phytoplankton community had a particularly low σ_{PSII} (<2.5 nm^2 $PSII^{-1}$) which did not present itself in anomalies in the other photophysiological parameters. The E_k in May was low in the Northern coastal zone and higher in offshore regions (Fig. 4k).

In August the F_v/F_m recovered across the Dutch North Sea (Fig. 4d). The σ_{PSII} was high in northern offshore region, and comparable to June in the rest of the Dutch North Sea (Fig. 4h). The E_k shows some interesting variability in August. The

regions off the Noordwijk coast and the of the Wadden Island coast were sampled twice, on two different times. These double measurements resulted in strongly different E_k, suggesting that time is a more important predictor in comparison to spatial variability.

5   To further investigate possible daily patterns we calculated standardized daily anomalies (z-scores). These show a clear diurnal trend in photosynthetic activity (Fig. 5). F_v/F_m is lowest during the middle of the day, while Ek, σ_{PSII} and $1/\tau$ peak during the day. As E_k is strongly correlated to P_{max} (Fig. S3), a clear daily pattern is also present in the photosynthetic electron transport rate.

Figure 4: Maps of the photophysiological parameters Fv/Fm (a-d), σ_{PSII} (e-h; in nm^2 PSII^{-1}) and E_k (i-l; in μmol photons m^{-2} s^{-1}) per month (from left to right: April, May, June and August). For more details on the location see Fig. 1.
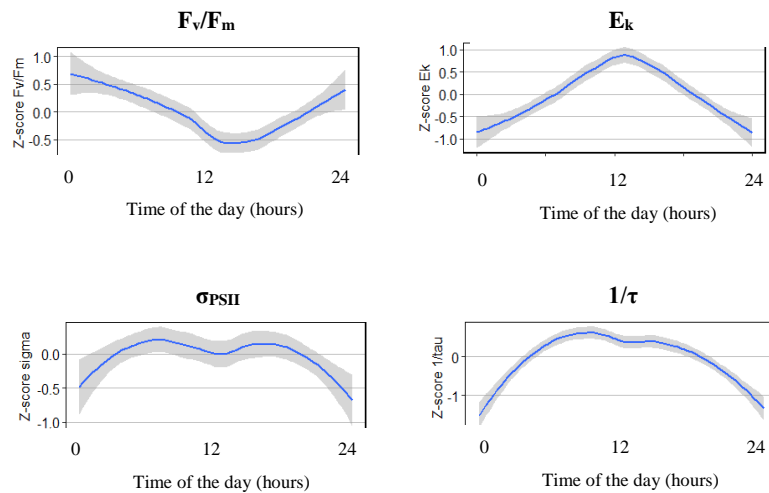
17

Figure 5: Standardized daily anomalies (z-scores) of F$_v$/F$_m$, E$_k$, σ$_{PSII}$ and 1/τ showing the diurnal trends in photophysiological data. On the x-axis the time of the day and on the y-axis the z-score.

3.5 Gross primary productivity

Gross primary productivity ranged from minimum 0.35 µg C L^{-1} h^{-1} in June to peak productivities of 602 µg C L^{-1} h^{-1} in the coastal zone in May (Fig. 6). The average GPP was highest in April and lowest in August. Monthly averages ranged from 116 ± 59 µg C L^{-1} h^{-1} in April and 8.7 ± 8.3 µg C L^{-1} h^{-1} in August, although these averages are not completely comparable due to different ship routes per month (Fig. 6). In April spatial heterogeneity in GPP was low. Highest rates in April were measured offshore (> 250 µg C L^{-1} h^{-1}) and in the coastal regions close to the Wadden Islands (Terschelling 10 in Fig. 1). In May, the GPP is heterogeneous without clear spatial pattern. Most production rates stay below 30 µg C L^{-1} h^{-1}, with local GPP peak rates over 600 µg C L^{-1} h^{-1} in the southern coastal zone. In June the Dutch North Sea was on average lower than in May, and showed slightly more large-scale spatial patterning. Highest values in June were observed (30-40 µg C L^{-1} h^{-1}) northwest of Noordwijk. In August GPP was low throughout the Dutch North Sea with the majority of water-column productivity rates staying below 10 µg C L^{-1} h^{-1}. In the southern coastal zone slightly higher rates were found, reaching up to 50 µg C L^{-1} h^{-1}.
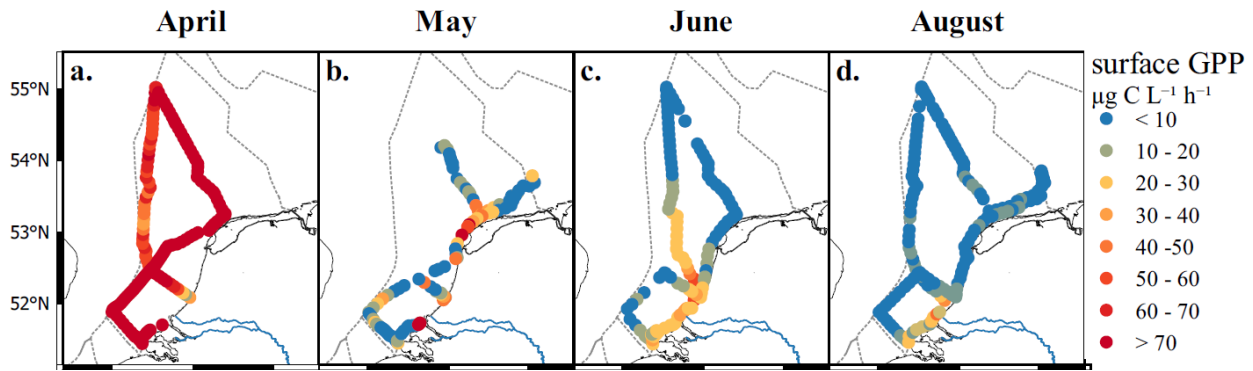
18

Figure 6: Gross primary productivity of the surface (a-d; in µg C L^{-1} h^1) per month (from left to right: April, May, June and August). Colors represent rates, where blue is low and red is high (see legend).

3.5 Spatial clustering

Strong collinearity between measured parameters was present. For spatial clustering these were removed based on the variable inflation factor (VIF>6; see supplementary material for pairplots), which resulted in removal of the photophysiological parameters P_{max}, α, a_{LHII}, n_{PSII}, the FCM-parameter of the total red fluorescence and the GPP. From the five defined phytoplankton groups (Table 2), the nano-crypto group was not used in the clustering because of collinearity (VIF>6). The remaining variables were the abundance of the remaining four FCM-defined phytoplankton groups (Pico-Red, Pico-Synecho, Nano-Red and Micro-Red), the total O/R ratio and five photophysiological parameters (F_v/F_m, $σ_{PSII}$, $1/τ$, [RCII], and E_k). For an overview of the collinearity between variables see the pairplots in the supplementary material.

Spectral cluster analysis resulted in identification of two to four clusters in each cruise. Most of these clusters were spatially separated and can therefore be seen as regions with distinct phytoplankton communities (Fig. 7). In April the clustering resulted in three clusters with a clear spatial pattern. In the PCA the variables that contributed most to the first principal component were all biomass related; [RCII] and a_{LHII}, related to the photosynthetic capacity per reaction center and per volume, and the abundance of the Nano-red group. The second principal component has photosynthetic parameters as two main contributors
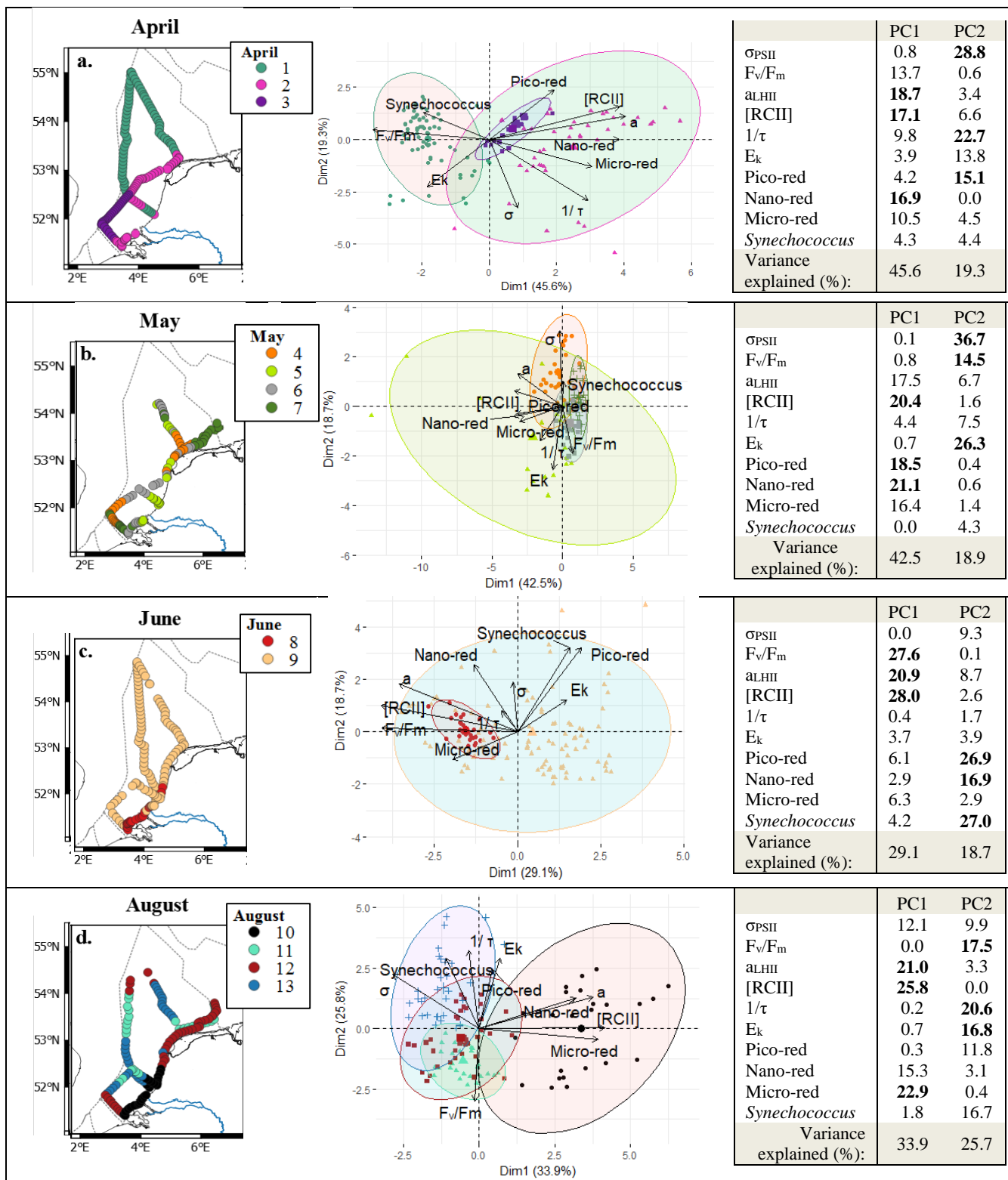
19

April

	PC1	PC2
σ_{PSII}	0.8	**28.8**
F_v/F_m	13.7	0.6
a_{LHII}	**18.7**	3.4
[RCII]	**17.1**	6.6
$1/\tau$	9.8	**22.7**
E_k	3.9	13.8
Pico-red	4.2	**15.1**
Nano-red	**16.9**	0.0
Micro-red	10.5	4.5
Synechococcus	4.3	4.4
Variance explained (%):	45.6	19.3

May

	PC1	PC2
σ_{PSII}	0.1	**36.7**
F_v/F_m	0.8	**14.5**
a_{LHII}	17.5	6.7
[RCII]	**20.4**	1.6
$1/\tau$	4.4	7.5
E_k	0.7	**26.3**
Pico-red	**18.5**	0.4
Nano-red	**21.1**	0.6
Micro-red	16.4	1.4
Synechococcus	0.0	4.3
Variance explained (%):	42.5	18.9

June

	PC1	PC2
σ_{PSII}	0.0	9.3
F_v/F_m	**27.6**	0.1
a_{LHII}	**20.9**	8.7
[RCII]	**28.0**	2.6
$1/\tau$	0.4	1.7
E_k	3.7	3.9
Pico-red	6.1	**26.9**
Nano-red	2.9	**16.9**
Micro-red	6.3	2.9
Synechococcus	4.2	**27.0**
Variance explained (%):	29.1	18.7

August

	PC1	PC2
σ_{PSII}	12.1	9.9
F_v/F_m	0.0	**17.5**
a_{LHII}	**21.0**	3.3
[RCII]	**25.8**	0.0
$1/\tau$	0.2	**20.6**
E_k	0.7	**16.8**
Pico-red	0.3	11.8
Nano-red	15.3	3.1
Micro-red	**22.9**	0.4
Synechococcus	1.8	16.7
Variance explained (%):	33.9	25.7

Figure 7: Overview of the spectral cluster analysis based on the non-collinear phytoplankton parameters (FCM: Pico-red, Nano-red, Micro-red, *Synechococcus*. FRRf: σ_{PSII}, F_v/F_m, a_{LHII}, $1/\tau$, E_k) separated per month (top to bottom: April, May, June and August). With on the left clusters visualized on maps and in the middle the bi-plots of the PCA of the data with confidence elipses per cluster (confidence 95%). In all graphics clusters are visualized by different colors as shown in the legend inset. Of the confidence elipses the border lines (and not the fill) correspond to the clusters. In the bi-plot overlapping conficence ellipses suggest a high similarity between groups while the size of the ellipse is a measure of variability within the group. On the right the table of the PCA analysis with contribution in % of the different variables, in bold the three variables that contribute most to the principal component.

(σ_{PSII} and $1/\tau$; 51.5%). Cluster one covers most of the Northern part of the Dutch North Sea, and a small part of the Noordwijk transect to the coast. The bi-plot of the PCA shows that the first cluster is negatively correlated to the main contributors of PC1 ([RCII] and a_{LHII}; Fig. 7), so this region consists a phytoplankton community with lower photosynthetic capacity per bulk and per volume. The coastal region is separated in two clusters, 2 and 3, with overlapping confidences ellipses (Fig. 7). The confidence interval of cluster 2 is larger than cluster 3, suggesting that the phytoplankton community in cluster 2 is more heterogeneous. Both clusters are positively correlated to the main contributors to PC1 ([RCII] and a_{LHII}), meaning this clusters consists of a community with higher photosynthetic capacity per volume.

In May the cluster analysis resulted in four different clusters, but without well-defined spatial pattern. The PCA biplots show that the confidence interval of cluster 5 overlaps most of the other clusters, indicating that this clusters has a weak support. E_k is negatively correlated with cluster 4 and σ_{PSII}, suggesting that cluster 4 contains low light acclimated algae. In contrast, in June only two clusters were found with a distinct separation between coastal and offshore phytoplankton communities. The PCA shows that the offshore phytoplankton community is consisting of a diverse phytoplankton community while the coastal phytoplankton community with high F_v/F_m and high a_{LHII} and [RCII]. The four clusters identified in August are spatially separated, but with some complications (Fig. 7). Different spatial clusters were appointed to the same region visited within a two-day time span twice; in the northeastern coastal region and at the transect of Noordwijk. Both times, cluster 11 is one of the overlapping spatial clusters. Cluster 11 corresponds to only nighttime sampling periods and is defined by low E_k and low $1/\tau$, indicative of a low light acclimated phytoplankton community. This suggests that cluster 11 is a temporal cluster instead of a spatial cluster. To test this we repeated the analysis for the month of August but only including the measurements performed within an 8 hour timeframe around noon (12:00±4h; see supplementary material Fig. S4). In this timeframe the southern coastal zone is distinct from the rest of the Dutch North Sea and corresponds to cluster 10 in the analysis of the complete dataset (Fig. 7d), so this cluster is defined by spatial variability. Cluster 12 and 13 are grouped together in the 12±4h timeframe as cluster 1. Cluster 11 is not recognized as cluster within the 12±4h timeframe, so seems indeed controlled by temporal rather than spatial variability.

4 Discussion

The aim of this study was to investigate spatial and seasonal patterns in photophysiological parameters, photosynthetic activity and phytoplankton biomass and composition with high spatial resolution. If successful, the method employed here can be further developed as novel monitoring method to improve existing monitoring programmes towards a more precise and ecosystemic ecological assessment (OSPAR, MSFD). The high-resolution methods used in this study, the FRRf and FCM, were able to visualize both the spatial and seasonal variability of the phytoplankton community in the Dutch North Sea. The strong seasonal dynamics in the Dutch North Sea affect the spatial distribution and community composition of the phytoplankton community (Baretta-Bekker et al., 2009; Brandsma et al., 2011). The typical spring bloom was partly captured by the cruise of April; nutrient concentration were generally still high, photophysiology uniform with and primary productivity high. At both the cruises in June and August primary productivity was low. The typical second late summer bloom period was covered by the cruises of this study, but an onset later than August is not unusual (Baretta-Bekker et al., 2009). In June and August phytoplankton populations were N-limited in a large part of the Dutch North Sea. This affects the community composition: Philippart et al. (2007) concluded that nutrient shifts were weakly correlated with biomass and more strongly with community structure. Generally, it is assumed that nutrient limitation favours small cell size, because of the higher surface to volume ratio of smaller cells. Fluctuating nutrient concentrations favour larger cells due to their greater maximum uptake rate and storage capacity (Stolte and Riegman, 1995; Giannini and Ciotti, 2016; Philippart et al., 2000), and the shift towards smaller species observed here using FCM is thus in accordance with this theory. This impacts the carrying capacity of the ecosystem, as microphytoplankton is a better food source for higher trophic levels than picophytoplankton. Picophytoplankton is more involved in the microbial food web, with less trophic efficiency and low contribution to carbon export (le Quéré et al., 2005). Flowcytometry is very suitable for such analyses. Even when species are identified by microscopy they are in analysis still grouped to size class (Philippart et al., 2007), a task the flowcytometer can do much faster. To understand the role of the phytoplankton in biogeochemical cyckes, the FCM clusters would ideally reflect taxonomic or functional groups, as calcifiers, silicifiers, DMS producers (such as *Phaeocystis*) and nitrogen fixers (le Quéré et al., 2005). The lack of identification of distinct clusters makes this sofar impossible. Other studies manually separate up to 10 phytoplankton groups with the same instrument (Marrec et al., 2018). These groups included Prochlorococcus, which is at the absolute limit of resolving capacity of the Cytosense FCM because of their small size and low fluorescence. They furthermore distinguished in the Pico-red between three groups based on FLO/FLR-ratio. They separated the nano-cryptophytes group two groups based on their orange fluorescence and included a microphytoplankton group with a size from 10 to 20 µm. These groups are still made up of many taxonomic genera and, apart from size, will not allow much for further interpretation of their role in the ecosystem or biogeochemical cycles. The same accounts for detection of nuisance phytoplankton; distinct clusters of toxic phytoplankton species are lacking. Although this will remain a challenge because toxicity in phytoplankton can differ within morphotypes and sometimes even differ per strain within a species (Tillman and Rick, 2003). But potentially, further research in flowcytometry can result in suspicious clusters to be flagged and further inspected by a specialist using microscopy. The

potential is certainly there, as much of the information retrieved by the FCM is still unexplored; the clustering is performed on totals (area under the peak) instead of the pulse-shape. This, in combination with more advanced camera options, may open up the possibility to further distinguish groups in the future.

5   Biomass might be one of the most important parameters to understand phytoplankton dynamics, but its direct measurement is not possible using high-resolution methods. Chlorophyll *a* concentration is often used as an estimate for biomass, although the Carbon:Chl *a* ratio is dependent on abiotic conditions and species-specific phenotypic plasticity (Flynn, 1991, 2005; Geider et al., 1997; Alvarez-Fernandez and Riegman, 2014; Halsey and Jones, 2015). Red fluorescence gave a good estimate of chlorophyll a concentration, both using the FRRf (adjusted $R^2 = 0.66$) and FCM (adjusted $R^2 = 0.90$). Both the FRRf and the
10   flowcytometer estimate the chlorophyll a concentration based upon the fluorescence in the red spectrum after excitation in the blue spectrum. There are some slight differences in the optics, the FRRf excites with a 450 nm LED and measures the fluorescence at 682 ± 30 nm, while the FCM excites at 488 nm and filters the red fluorescence over a longpass 650 nm filter towards the red fluorescence detector. The smaller detection range of the FRRf detector is optimized around the maximum emission of PSII and limits contamination by PSI (Franck et al., 2002; Oxborough et al., 2012). The second difference is the
15   fluorescent state of the photosystems, the strong laser of the flowcytometer can only measure the maximum fluorescence (F_m), which is a parameter more prone to quenching than the minimum fluorescence measured by the FRRf. Yet, the biggest difference concerns the method; where the flowcytometer measures the fluorescence per particle, the FRRf does only a bulk measurement. In a bulk measurement other particles in solution scatter the excitation and emission photons, plus the emitted fluorescence of the phytoplankton is subject to reabsorption, especially at higher biomass densities. The latter seems to have
20   the most impact on chlorophyll a concentrations, as the fit of the flowcytometer derived red fluorescence is a better than the FRRf minimum fluorescence. Other studies that use the FCM to estimate chlorophyll a concentrations also showed good relationships, but find better fits using the bulk measurements using a fluorimeter (Thyssen et al., 2015; Marrec et al., 2018). The conversion to biomass may also be done from cell abundances. Some studies use the oversimplified assumption that all cells have a spherical shape and a constant C content per biovolume (Tarran et al., 2006). With the scanning flowcytometer it
25   is also possible to estimate biovolume based on scattering properties of the cell, but this relationship appears to be taxon specific (Rijkeboer, pers. comm.). This relationship will be further explored by comparing the calculated biovolume based on the Image in Flow pictures and the flowcytometric properties of these phytoplankters.

Phytoplankton biomass does not necessarily reflect primary productivity, as high grazing pressure can keep biomass low while
30   production is high. This is clearly visualized by the lack of resemblance between patterns in cell numbers (Fig. 3 a-d) and primary productivity (Fig. 6). Fast Repetition Rate fluorometry offers insight into the light acclimation, light use efficiency and the primary productivity of the phytoplankton, but interpretation of photophysiological parameters is not straightforward and requires algorithms that are subject to constant revision (Oxborough et al., 2012; Lawrenz et al., 2013). One of the most commonly used parameters is F_v/F_m, the quantum efficiency of PSII. F_v/F_m decreases at limiting nutrient conditions or other

23

abiotic stressors (Suggett et al., 2009b; Kolber et al. 1988; Kolber and Falkowski, 1993; Beardall et al. 2001; Ly et al. 2014). In this study a large part of the Dutch North Sea shifted from nutrient sufficiency to nutrient limitation between April and May, which was reflected in the low efficiency of PSII (F_v/F_m; Fig. 4). The F_v/F_m recovered between May and June, which suggest that the phytoplankton adapted to nutrient limiting conditions (Kruskopf and Flynn, 2005). However, photophysiological parameters are also varying per taxonomic group; smaller taxa typically have lower F_v/F_m values and higher σ_{PSII} values (Kolber et al., 1988; Suggett et al., 2009b). Indeed, by flowcytometry we find that the biggest shift in community composition took place between May and June from a nanophytoplankton dominated community to a picophytoplankton dominated community. These findings demonstrate how flowcytometry and fast repetition rate fluorometry can supplementary improve ecosystem understanding.

Regarding the use of photophysiology in a monitoring program, the diurnal variability is a factor to be aware of. Diurnal trends make extrapolation of rates obtained at a specific timepoint to daily rates difficult. Most photophysiological parameters we measured showed diurnal trends (Fig. 5). The diurnal trend is dictated by the phytoplankton cell cycle, a circadian oscillator and photophysiological response to varying irradiance (Suzuki and Johnson, 2001; Cohen and Golden, 2015; Schuback et al., 2016). Phytoplankton uses photophysiological plasticity responses to minimize photodamage and optimize growth under fluctuating irradiance (Schuback et al., 2016; Behrenfeld et al., 2002). The diurnal variability is also reflected in the gross primary productivity estimations because also the electron requirement for carbon fixation is subject to diurnal variation (Schuback et al., 2016; Lawrenz et al., 2013; Raateoja, 2004). To interpret spatial variability separately from temporal variability and to provide a more reliable estimate of gross primary productivity, Schuback et al. (2016) suggest a correction with normalized Stern-Volmer quenching (NPQ_{NSV}), which needs further research. A monitoring program including photophysiology should account for diurnal variability, for example by using only measurements collected in a certain timeframe or the effect should be quantified by using a Lagrangian approach where the photosynthetic activity of the same population is followed during the day.

The reliability of variable fluorescence as estimate of gross primary productivity is depending on many cell processes from the photon absorbance to carbon assimilation. The variable fluorescence reflects the first step of photosynthesis; the efficiency of which photons are captured and electrons produced and transferred. However, to interpret gross primary productivity in an ecological or biogeochemical meaningful way, the FRR units of electrons per unit time need to be converted to carbon units. Gross photosynthesis correlates well with photosynthetic oxygen evolution (Suggett et al., 2003), and multiple studies have shown good correlation between ^{14}C-derived estimates of primary productivity and FRRf-derived estimates using a constant conversion factor (Melrose et al., 2006; Kromkamp et al., 2008). However, in reality this parameter is not a constant, as along the pathway from electron to carbon atom electrons are consumed by other cell processes (Flameling and Kromkamp, 1998; Halsey and Jones, 2015; Schuback et al., 2016). Therefore, a reliable GPP estimate in carbon units from FRR fluorometry requires more research and estimates provide relative rather than qualitative values. Despite its limitations the fact that the

method can measure *in situ*, with relatively little phytoplankton manipulation before measurement, makes the method promising. Calibration with other methods, such as concurrent C14 of C13 incubations, could help to better understand the processes from electron excitation to carbon fixation. However, it should be recognized that these types of measurements come with their own problems, and measure something in between net and gross primary productivity depending on the incubation time and growth rate of the phytoplankton (Halsey and Jones, 2015). So it remains a question which method is measuring the 'real' primary productivity. Attempts to calculate primary productivity from flowcytometer data have also been made, which is actually based on the diurnal cycle in cell size caused by cell division (Marrec et al., 2018). Despite the limitations of GPP estimates by variable fluorescence, our results clearly show large spatial variability in gross primary production concurrent to the expected strong variability during the growth season. This spatial heterogeneity is not fully captured by sampling at the standard low-resolution monitoring stations, showing the added value of our approach. Primary productivity was highest in April, and relatively large values were also observed offshore, indicating that a low phytoplankton biomass does not necessarily means that primary production is low. Our GPP rates were based on the same electron requirement for C-fixation ($\Phi_{e,C}$). However, this is a likely oversimplification as $\Phi_{e,C}$ is known to vary with abiotic conditions (Lawrenz et al., 2013) and the changes in nutrient conditions and temperature during the growth season are likely to affect GPP. This will be the topic of a future publication and we expect that the detection of several biogeographic regions will help us in predicting $\Phi_{e,C}$.

Biogeographic regions

The applied automated cluster methods were a useful tool to roughly identify distinct phytoplankton communities or distinct biogeographic regions. The spectral clustering method used in this study was originally designed to detect phytoplankton blooms and understanding the involved dynamics (Rousseeuw et al., 2015; Lefebvre and Poisson-Caillault, in press). In this study this method was applied to identify different phytoplankton communities and observe spatial patterns. In some months, like April and June, it was indeed possible to identify regions with distinct phytoplankton communities. In other months, such as May, the clustering was not clearly regional but heterogeneous over the whole Dutch North Sea. A clear distinction between phytoplankton communities of the coastal zone and off-shore regions could be made in all months, except May. Unfortunately, the model was not able to automatically visualize all spatial heterogeneity. For instance, in April off the coast from Terschelling we found a distinct community with high cryptophyte abundance not resulting in a separate cluster. Additionally, temporal variation (i.e. day-night differences) was interfering with the spatial clustering in August. So although such models are useful for visualization and following changes in spatial heterogeneity, input and output need to be critically evaluated before implementation in monitoring programs. To test whether the differences between months result from seasonal variation or other factors, results over multiple years and additional seasonal cruises need to be made to better characterize heterogeneity of the phytoplankton community structure.

Designing 'smart' phytoplankton monitoring

A smart monitoring program combines high and low resolution methods in a supplementary way. No method or parameters will offer clear-cut answers, which accounts for low-resolution and high-resolution methods alike. Low resolution methods remain a necessity to support the proposed measurements set-up for three reasons: the practical requirement for calibration and blank correction, to retrieve more detailed taxonomical information and to capture the variability in the water column. Firstly, FRRf measurements are affected by interference of colored dissolved matter which can lead to under or overestimation of some parameters (like F_v/F_m; Cullen and Davis, 2003). The blank correction is still manual and should be done at least when abiotic conditions change.

Secondly, regular measurements of the whole water column remain a necessity to retrieve information on the vertical heterogeneity and the light extinction in the water column. Surface water measurements are only a good reflection of the water column when mixed layer depth is deeper than the euphotic zone. Stratification or mixed layer depth shallower than the euphotic zone can result in subsurface chlorophyll maximum layers and significantly different phytoplankton community (Latasa et al., 2017). Extrapolation of surface measurements to water column estimates is required to assess the carrying capacity of the ecosystem and the contributions to biogeochemical cycles. Both the mixed layer depth and the light extinction in the water column can only be determined by frequent CTD casts equipped with PAR sensor.

Thirdly, the level of detail required to identify harmful, keystone or invasive species is only achieved by microscopy analysis. A potential combination of high and low resolution methods would be to use high-resolution methods to identify extra sampling points based on real-time projections, opening up early warning methodologies. For example, in the April cruise both Noordwijk 70 and Terschelling 235 km show high gross primary productivity, but in between both high and low productivity rates occur which are not detected with the current sampling program (Fig. 6). The combination of high-resolution *in situ* methods with remote sensing has potential to further increase the spatial and temporal scale. Estimating biological parameters using remote sensing is still difficult, especially in turbid, coastal, case-2 waters (Gohin et al., 2005; van der Woerd et al., 2008). Therefore, *in vivo* measurements are required to calibrate remote sensing based models and we suggest that automated flowcytometry and production measurements based on FRRf methodology can fulfil this role.

5 Conclusions

A good monitoring program monitors the presence of functional types of phytoplankton, including the harmful taxons, the carrying capacity of the ecosystem and changes in biogeochemical cycling. The objective of this study was to evaluate the use of FRR fluorometry and flowcytometry for such monitoring purposes. The four conducted cruises spread over 5 months offered a wide variety of environmental conditions and phytoplankton community states, which the utilized methods were able to visualize. Inclusion of high-resolution methods in monitoring programs allows for analysis of finer scale events. Furthermore, it allows for analysis of living phytoplankton and is thereby able to measure rates and avoid effects of preservation and storage of samples. Another advantage is that high-resolution methods allows for easier comparison

between countries, once common protocols have been established. Nevertheless, low resolution methods remain a necessity for more detailed taxonomic analysis, information on vertical heterogeneity, to calibrate and to correct for blanks. Data analysis might be the biggest bottleneck of the implementation of these high-resolution methods. The cluster analysis of flowcytometric data has high potential for improvement to increase the informative value of the method. Especially identification of phytoplankton clusters with a functional quality, such as nitrogen fixers, calcifiers or DMS-producers, would be helpful for interpretation of ecosystem dynamics and biogeochemical fluxes. Regarding the FRRf, the main challenge is converting electron transport rate to gross primary productivity in carbon units. Further research in these topics would benefit implementation of these methods into monitoring protocols. Furthermore, it is important to account for diurnal patterns in monitoring set-up to be able to distinguish between diurnal and spatial variability. Possibly the diurnal variability could be modelled, but more studies with a Langragian based approach would be needed for a better understanding of the impact of diurnal variability in the data. Overall, the in this study presented high-resolution measurement set-up has large potential to improve phytoplankton monitoring in supplement to existing low-resolution monitoring programs.

References

Alvarez-Fernandez, S., and Riegman, R. (2014). Chlorophyll in North Sea coastal and offshore waters does not reflect long term trends of phytoplankton biomass. Journal of Sea Research, 91, 35–44. https://doi.org/10.1016/j.seares.2014.04.005

Baretta-Bekker, J.G., Baretta, J.W., Latuhihin, M.J., Desmit, X., and Prins, T.C. (2009). Description of the long-term (1991-2005) temporal and spatial distribution of phytoplankton carbon biomass in the Dutch North Sea. Journal of Sea Research, 61(1–2), 50–59. https://doi.org/10.1016/j.seares.2008.10.007

Beardall, J., T. Berman, P. Heraud, M. O. Kadiri, B. R. Light, G. Patterson, S. Roberts, B. Sulzberger, E. Sahan, U. Uehlinger, and B. Wood. (2001). A comparison of methods for detection of phosphate limitation in microalgae. Aquatic Sciences **63**:107-121.

Behrenfeld, M.J., Maranon, E., Siegel,D.A., Hooker, S.B. (2002). Photoacclimation and nutrient-based model of light-saturated photosynthesis for quantifying oceanic primary production. *Mar. Ecol. Prog. Ser.*,228:103-117

Behrenfeld, M. J., O'Malley, R. T., Siegel, D. A., McClain, C. R., Sarmiento, J. L., Feldman, G. C., Milligan, A.J., Falkowski, P.G., Letelier, R.M., Boss, E. S. (2006). Climate-driven trends in contemporary ocean productivity. Nature, 444(7120), 752–755. https://doi.org/10.1038/nature05317

Brandsma, J., Hopmans, E. C., Philippart, C. J. M., Veldhuis, M. J. W., Schouten, S., Sinninghe Damsté, J. S. (2011). Low temporal variation in the intact polar lipid composition of North Sea coastal marine water reveals limited chemotaxonomic value. Biogeosciences, 9(3), 1073–1084. https://doi.org/10.5194/bg-9-1073-2012

Burson, A., Stomp, M., Akil, L., Brussaard, C. P. D., and Huisman, J. (2016). Unbalanced reduction of nutrient loads has created an offshore gradient from phosphorus to nitrogen limitation in the North Sea, 869–888. https://doi.org/10.1002/lno.10257

Capuzzo, E., Stephens, D., Silva, T., Barry, J., Forster, R. M. (2015). Decrease in water clarity of the southern and central North Sea during the 20th century. Global Change Biology, 21(6), 2206–2214. https://doi.org/10.1111/gcb.12854

Capuzzo, E., Lynam, C. P., Barry, J., Stephens, D., Forster, R. M., Greenwood, N., McQuatters-Gollop, A., Silva, T., van Leeuwen, S.M., Engelhard, G. H. (2017). A decline in primary production in the North Sea over 25 years, associated with reductions in zooplankton abundance and fish stock recruitment. Global Change Biology, 1–13. https://doi.org/10.1111/gcb.13916

Cloern, J.E., Foster, S.Q. and Kleckner, A.E. (2014). Phytoplankton primary production in the world's estuarine-coastal ecosystems. Biogeosciences, 11(9), 2477–2501. https://doi.org/10.5194/bg-11-2477-2014

Cohen, S.E. and Golden, S.S. (2015). Circadian Rhythms in Cyanobacteria. Microbiol Mol Biol Rev. 79(4):373-85. 10.1128/MMBR.00036-15.

Cullen, J.J., and Davis, R.F. (2001). The blank can make a big difference in oceanographic measurements. Limnol. Oceanogr. Bulletin, 12(2), 29–35.

Falkowski, P. and Kiefer, D.A. (1985). Chlorophyll a fluorescence in phytoplankton: relationship to photosynthesis and biomass. Journal of Plankton Research, 7(5), 715–731.

5 Falkowski, P.G. (1998). Biogeochemical Controls and Feedbacks on Ocean Primary Production. Science, 281(5374), 200–206. https://doi.org/10.1126/science.281.5374.200

Flameling, I.A. and J. Kromkamp (1998). Light dependence of quantum yields for PSII charge separation and oxygen evolution in eukaryotic algae. Limnology and Oceanography. 43:284-297

10 Flynn, K.J. 1991. Algal carbon-nitrogen metabolism: a biochemical basis for modelling the interactions between nitrate and ammonium uptake. Journal.of.Plankton.Research. 13:373-387.

Flynn, K.J. 2005. Modelling marine phytoplankton growth under eutrophic conditions. Journal of Sea Research 54:92-103.

15 Franck, F., Juneau, P., and Popovic, R. (2002). Resolution of the Photosystem I and Photosystem II contributions to chlorophyll fluorescence of intact leaves at room temperature. Biochimica et Biophysica Acta - Bioenergetics, 1556(2–3), 239–246. https://doi.org/10.1016/S0005-2728(02)00366-3

20 Geider, R.J., MacIntyre, H.L. and Kana, T. M. (1997). Dynamic model of phytoplankton growth and acclimation: responses of the balanced growth rate and the chlorophyll a:carbon ratio to light, nutrient-limitation and temperature. Marine Ecology Progress Series 148:187-200.

Giannini, M.F.C., Ciotti, Á M. (2016). Parameterization of natural phytoplankton photo-physiology: Effects of cell size and nutrient concentration. Limnology and Oceanography, 61(4), 1495–1512. https://doi.org/10.1002/lno.10317

25

Gohin, F., Loyer, S., Lunven, M., Labry, Froidefond, C.J.M., Delmas, D., Huret M. and Herbland. A. 2005. Satellite-derived parameters for biological modelling in coastal waters: Illustration over the eastern continental shelf of the Bay of Biscay, Remote Sensing of Environment 95: 29-46.

30 Goss, R., Ann Pinto, E., Wilhelm, C., Richter, M. (2006). The importance of a highly active and ΔpH-regulated diatoxanthin epoxidase for the regulation of the PS II antenna function in diadinoxanthin cycle containing algae. Journal of Plant Physiology, 163(10), 1008–1021. https://doi.org/10.1016/j.jplph.2005.09.008

Halsey, K. H., & Jones, B. M. (2015). Phytoplankton Strategies for Photosynthetic Energy Allocation. Annu. Rev. Mar. Sci. 2015. 7:265–97 , https://doi.org/10.1146/annurev-marine-010814-015813

Kassambara, A. and Mundt, F., 2017. factoextra: Extract and Visualize the Results of Multivariate Data Analyses. R package version 1.0.5. https://CRAN.R-project.org/package=factoextra

Kolber, Z., Zehr, J., Falkowski, P.G. (1988). Effects of growth irradiance and nitrogen limitation on photosynthetic energy conversion in photosystem II. Plant Physiology. 88:923-929.

Kolber, Z. and Falkowski, P.G. (1993). Use of active fluorescence to estimate phytoplankton photosynthesis in situ. Limnology and Oceanography. **38**:1646-1665.

Kolber, Z.S., Prášil, O., Falkowski, P.G. (1998). Measurements of variable chlorophyll fluorescence using fast repetition rate techniques: Defining methodology and experimental protocols. Biochimica et Biophysica Acta - Bioenergetics, 1367(1–3), 88–106. https://doi.org/10.1016/S0005-2728(98)00135-2

Kromkamp, J.C., and Forster, R.M. (2003). The use of variable fluorescence measurements in aquatic ecosystems: differences between multiple and single turnover measuring protocols and suggested terminology. European Journal of Phycology, 38(2), 103–112. https://doi.org/10.1080/0967026031000094094

Kromkamp, J. C., Dijkman, N. A., Peene, J., Simis, S. G. H., Gons, H. J. (2008). Estimating phytoplankton primary production in Lake IJsselmeer (The Netherlands) using variable fluorescence (PAM-FRRF) and C-uptake techniques Estimating phytoplankton primary production in Lake IJsselmeer (The Netherlands) using variable fluoresce, 262. https://doi.org/10.1080/09670260802080895

Kromkamp, J.C., and Van Engeland, T. (2010). Changes in phytoplankton biomass in the western Scheldt estuary during the period 1978-2006. Estuaries and Coasts, 33(2), 270–285. https://doi.org/10.1007/s12237-009-9215-3

Kruskopf, M. and Flynn, K.J. (2005). Chlorophyll content and fluorescence responses cannot be used to gauge reliably phytoplankton biomass, nutrient status or growth rate. New Phytologist **169**:525-536.

Latasa, M., Cabello, A.M., Morán, X.A.G., Massana, R. and Scharek, R. (2017). Distribution of phytoplankton groups within the deep chlorophyll maximum, Limnol. Oceanogr., 62: 665-685.

Lawrenz, E., Silsbe, G., Capuzzo, E., Ylöstalo, P., Forster, R.M., Simis, S.G.H., Prášil, O., Kromkamp, J.C., Hickman, A.E., Moore, C.M., Forget, M.H., Geider, R.J., Suggett, D.J. (2013). Predicting the Electron Requirement for Carbon Fixation in Seas and Oceans. PLoS ONE, 8(3). https://doi.org/10.1371/journal.pone.0058137

Lefebvre A., Poisson-Caillault E., In press. High resolution overview of phytoplankton spectral groups and hydrological conditions in the eastern English Channel using unsupervised clustering. Marine Ecology Progress Series. https://doi.org/10.3354/meps12781.

Ly, J., C. J. M. Philippart, and J. C. Kromkamp. 2014. Phosphorus limitation during a phytoplankton spring bloom in the western Dutch Wadden Sea. Journal of Sea Research **88**:109-120.

Marinov, I., Doney, S.C., and Lima, I.D. (2010). Response of ocean phytoplankton community structure to climate change over the 21st century: partitioning the effects of nutrients, temperature and light. Biogeosciences, 7(12), 3941–3959. https://doi.org/10.5194/bg-7-3941-2010

Marrec, P., Doglioli, A.M., Grégori, G., Dugenne, M., Della Penna, A., Bhairy, N., Cariou, T., Hélias Nunige, S., Lahbib, S., Rougier, G., Wagener, T., Thyssen, M. (2017). Coupling physics and biogeochemistry thanks to high resolution observations of the phytoplankton community structure in the North-Western Mediterranean Sea. Biogeosciences Discussions, (August), 1–54. https://doi.org/10.5194/bg-2017-343

Melrose, D.C., Oviatt, C.A., O'Reilly, J.E., Berman, M.S. (2006). Comparisons of fast repetition rate fluorescence estimated primary production and 14C uptake by phytoplankton. Marine Ecology Progress Series, 311, 37–46. https://doi.org/10.3354/meps311037

Montes-Hugo, M., Doney, S. C., Ducklow, H. W., Fraser, W., Martinson, D., Stammerjohn, S. E., and Schofield, O. (2009). Recent Changes in Phytoplankton Communities Associated with Rapid Regional Climate Change Along the Western Antarctic Peninsula. Science, 323(5920), 1470–1473. https://doi.org/10.1126/science.1164533

Moore, C. M., Suggett, D. J., Hickman, a. E., Kim, Y.-N., Tweddle, J. F., Sharples, J., Geider, R.J., Holligan, P.M. (2006). Phytoplankton photoacclimation and photoadaptation in response to environmental gradients in a shelf sea, Limnol. Oceanogr. 44(0), 1–46. https://doi.org/10.4319/lo.2006.51.2.0936

Oxborough, K., Moore, C.M., Suggett, D.J., Lawson, T., Chan, H.G., Geider, R.J. (2012). Direct estimation of functional PSII reaction center concentration and PSII electron flux on a volume basis : a new approach to the analysis of Fast Repetition Rate fluorometry (FRRf) data, OCEANOGRAPHY: METHODS,142–154. https://doi.org/10.4319/lom.2012.10.142

5   Peeters, J. and Peperzak, L. (1990). Nutrient limitation in the North Sea: a bioassay approach. Netherlands Journal of Sea Research, 26(1), 61–73. https://doi.org/10.1016/0077-7579(90)90056-M

Philippart, C. J. M., Cade, G. C., Raaphorst, W. Van, & Riegman, R. (2000). Long-term phytoplankton – nutrient interactions in a shallow coastal sea: Algal community structure, nutrient budgets, and denitrification potential. Limnol. Oceanogr., 45(1),
10   131–144.

Philippart, C. J. M., Beukema, J. J., Cadée, G. C., Dekker, R., Goedhart, P. W., Van Iperen, J. M., Leopold, M.F. Herman, P. M. J. (2007). Impacts of nutrient reduction on coastal communities. Ecosystems, 10(1), 95–118. https://doi.org/10.1007/s10021-006-9006-7

15

Philippart, C. J. M., Anadón, R., Danovaro, R., Dippner, J. W., Drinkwater, K. F., Hawkins, S. J., Oguz, T., O'Sullivan, G., Reid, P. C. (2011). Impacts of climate change on European marine ecosystems: Observations, expectations and indicators. Journal of Experimental Marine Biology and Ecology, 400(1–2), 52–69. https://doi.org/10.1016/j.jembe.2011.02.023

20   Poisson-caillault, E. and Ternynck, P (2016). uHMM: Construct an Unsupervised Hidden Markov Model. R Package version 1.0, https://cran.r-project.org/package=uhmm

Quéré, C. Le, Harrison, S. P., Colin Prentice, I., Buitenhuis, E. T., Aumont, O., Bopp, L., Claustre, H., Cotrim Da Cunha, L., Geider, R.J., Giraud, X., Klaas, C., Kohfeld, K.E., Legendre, L., Manizza, M., Platt, T., Rivkin, R.B., Sathyendranath, S., Uitz,
25   J., Watson, A.J., Wolf-Gladrow, D. (2005). Ecosystem dynamics based on plankton functional types for global ocean biogeochemistry models\rdoi:10.1111/j.1365-2486.2005.1004.x. Global Change Biology, 11(11), 2016–2040. https://doi.org/10.1111/j.1365-2486.2005.01004.x

Raateoja, M. P. (2004). Fast repetition rate fluorometry (FRRF) measuring phytoplankton productivity: A case study at the
30   entrance to the Gulf of Finland, Baltic Sea. Boreal Env. Res. 9: 263–276.

Rantajärvi, E., Olsonen, R., Hällfors, S., Leppänen, J. M., and Raateoja, M. (1998). Effect of sampling frequency on detection of natural variability in phytoplankton: Unattended high-frequency measurements on board ferries in the Baltic Sea. ICES Journal of Marine Science, 55(4), 697–704. https://doi.org/10.1006/jmsc.1998.0384

Rijkeboer, M. (2018). Automated characterization of phytoplankton community into size and pigment groups based on flow cytometry. MEM 2018-20. RWS Information pp.18

5   Rousseeuw, K., Poison Caillault, E., Lefebvre, A., Hamad, D. (2015). Achimer Hybrid hidden Markov model for marine environment monitoring. IEEE Journal Of Selected Topics In Applied Earth Observations And Remote Sensing, 8(1), 204–213. https://doi.org/http://dx.doi.org/10.1109/JSTARS.2014.2341219

Rutten, T. (2015). Evaluatie testen van diverse CytoSense configuraties. TRP2015.001, 32 pp (in Dutch)

10

Sarmiento, J.L., Slater, R., Barber, R., Bopp, L., Doney, S.C., Hirst, A.C., Kleypas, J., Matear, R., Mikolajewicz, U., Monfray, P., Soldatov, V., Spall, S. a. Stouffer, R. (2004). Response of ocean ecosystems to climate warming. Global Biogeochem. Cycles, 18(3), GB3003. https://doi.org/10.1029/2003GB002134

15   Schiebel, R., Spielhagen, R. F., Garnier, J., Hagemann, J., Howa, H., Jentzen, A., Martínez-Garcia, A., Meiland, J., Michel, E., Repschläger, J., Salter, I., Yamasaki, M., Haug, G. (2017). Modern planktic foraminifers in the high-latitude ocean. Marine Micropaleontology, 136, 1–13. https://doi.org/10.1016/j.marmicro.2017.08.004

Seadatanet (2018). SeaDataCloud Flow Cytometry Standardised Cluster Names. Natural Environment Research Council.
20   Version 3. http://vocab.nerc.ac.uk/collection/F02/current/F0200007/

Sieburth J.M., Smetacek, V., Lenz, J. (1978). Pelagic ecosystem structure: heterotrophic compartments of the plankton and their relationship to plankton size fractions. Limnol Oceanogr 23:1256–1263

25   Schuback, N., Flecken, M., Maldonado, M. T., Tortell, P. D. (2016). Diurnal variation in the coupling of photosynthetic electron transport and carbon fixation in iron-limited phytoplankton in the NE subarctic Pacific. Biogeosciences, 13(4), 1019–1035. https://doi.org/10.5194/bg-13-1019-2016

Sündermann, J., and Pohlmann, T. (2011). A brief analysis of North Sea physics. Oceanologia, 53(3), 663–689.
30   https://doi.org/10.5697/oc.53-3.663

Silsbe, G.M. and Kromkamp, J.C. (2012). Modeling the irradiance dependency of the quantum efficiency of photosynthesis. Limnology and Oceanography: Methods, 10(9), 645–652. https://doi.org/10.4319/lom.2012.10.645

35   Silsbe, G.M., Oxborough, K., Suggett, D.J., Forster, R.M., Ihnken, S., Komárek, O., Lawrenz E., Prášil, O., Röttgers, R., Šicner, M., Simis, S.G.H., Van Dijk, M., Kromkamp, J.C. (2015). Toward autonomous measurements of photosynthetic

electron transport rates: An evaluation of active fluorescence-based measurements of photochemistry. Limnology and Oceanography: Methods, 13(3), 138–155. https://doi.org/10.1002/lom3.10014

Silsbe, G.M., Behrenfeld, M.J., Halsey, K.H., Milligan, A.J., Westberry, T.K. (2016). The CAFE model: A net production model for global ocean phytoplankton. Global Biogeochemical Cycles, 30(12), 1756–1777. https://doi.org/10.1002/2016GB005521

Smyth, T.J., Pemberton, K.L., Aiken, J., Geider, R.J. (2004). A methodology to determine primary production and phytoplankton photosynthetic parameters from Fast Repetition Rate Fluorometry. Journal of Plankton Research, 26(11), 1337–1350. https://doi.org/10.1093/plankt/fbh124

Suggett, D.J., Oxborough, K., Baker, N.R., MacIntyre, H.L., Kana, T. M., Geider, R.J. (2003). Fluorescence Measurements for Assessment of Photosynthetic Electron Transport in Marine Phytoplankton. European Journal of Phycology, 38(4), 371–384. https://doi.org/10.1080/09670260310001612655

Suggett, D.J., MacIntyre, H.L., Kana, T. M., Geider, R.J. (2009a). Comparing electron transport with gas exchange: Parameterising exchange rates between alternative photosynthetic currencies for eukaryotic phytoplankton. Aquatic Microbial Ecology, 56(2–3), 147–162. https://doi.org/10.3354/ame01303

Suggett, D.J., C.M. Moore, A E. Hickman, and R.J. Geider. (2009b). Interpretation of fast repetition rate (FRR) fluorescence: signatures of phytoplankton community structure versus physiological state. Marine Ecology-Progress Series **376**:1-19.

Suzuki, L., and Johnson, C. H. (2001). Minireview Algae Know the Time of Day: Circadian and Photoperiodic Programs 1, 942(May), 933–942.

Stolte, W., and Riegman, R. (1995). Effect of phytoplankton cell size on transient- state nitrate and ammonium uptake kinetics. Microbiology, 141(1995), 1221–1229.

Sündermann, J., and Pohlmann, T. (2011). A brief analysis of North Sea physics. Oceanologia, 53(3), 663–689. https://doi.org/10.5697/oc.53-3.663

Tarran, G.A., Heywood, J.L., and Zubkov, M.V. (2006). Latitudinal changes in the standing stocks of nano- and picoeukaryotic phytoplankton in the Atlantic Ocean. Deep-Sea Research Part II: Topical Studies in Oceanography, 53(14–16), 1516–1529. https://doi.org/10.1016/j.dsr2.2006.05.004

Thyssen, M., Alvain, S., Dessailly, D., Rijkeboer, M., Guiselin, N., Creach, V. (2015). High-resolution analysis of a North Sea phytoplankton community structure based on in situ flow cytometry observations and potential implication for remote sensing, Biogeosciences, 12, 4051–4066. https://doi.org/10.5194/bg-12-4051-2015

Tillmann, U., and Rick, H.J. (2003). North Sea phytoplankton: A review. Senckenbergiana Maritima, 33(1–2), 1–69. https://doi.org/10.1007/BF03043047

Van der Woerd, H. J. and R. Pasterkamp. 2008. HYDROPT: A fast and flexible method to retrieve chlorophyll-a from multispectral satellite observations of optically complex coastal waters, Remote Sensing of Environment, 112: 1795-1807.

Vaulot, D., Eikrem W., Viprey, M., Moreau, H. (2008). The diversity of small eukaryotic phytoplankton (< or =3 micron) in marine ecosystems. FEMS Microbiol Rev 32:795–820

Webb, W.L., Newton, M., Starr, D. (1974). Carbon dioxide exchange of *Alnus rubra*: a mathematical model. Oecologia. **17**:281-291.

Wickham, H., 2009. ggplot2: Elegant Graphics for Data Analysis. Springer-Verlag New York

Zuur, A.F., Ieno, E.N., Walker, N., Saveliev, A.A., and Smith, G.M. (2009). Mixed effects models and extensions in ecology with R. Springer